Redox Biology 58 (2022) 102533

Contents lists available at ScienceDirect

Redox Biology

journal homepage: www.elsevier.com/locate/redox

Mitochondria-originated redox signalling regulates KLF-1 to promote longevity in *Caenorhabditis elegans*

Johannes CW Hermeling [a,b], Marija Herholz [a,b], Linda Baumann [a,b], Estela Cepeda Cores [a,b], Aleksandra Zečić [a,b], Thorsten Hoppe [a,c,d], Jan Riemer [a,e], Aleksandra Trifunovic [a,b,c,*]

[a] *Cologne Excellence Cluster on Cellular Stress Responses in Ageing-Associated Diseases (CECAD), Germany*
[b] *Institute for Mitochondrial Diseases and Ageing, Medical Faculty, University of Cologne, Cologne, D-50931, Germany*
[c] *Center for Molecular Medicine Cologne (CMMC), Cologne, D-50931, Germany*
[d] *Institute for Genetics, University of Cologne, Cologne, D-50674, Germany*
[e] *Institute for Biochemistry, University of Cologne, Cologne, D-50931, Germany*

A B S T R A C T

Alternations of redox metabolism have been associated with the extension of lifespan in roundworm *Caenorhabditis elegans*, caused by moderate mitochondrial dysfunction, although the underlying signalling cascades are largely unknown. Previously, we identified transcriptional factor Krüppel-like factor-1 (KLF-1) as the main regulator of cytoprotective longevity-assurance pathways in the *C. elegans* long-lived mitochondrial mutants. Here, we show that KLF-1 translocation to the nucleus and the activation of the signalling cascade is dependent on the mitochondria-derived hydrogen peroxide (H_2O_2) produced during late developmental phases where aerobic respiration and somatic mitochondrial biogenesis peak. We further show that mitochondrial-inducible superoxide dismutase-3 (SOD-3), together with voltage-dependent anion channel-1 (VDAC-1), is required for the life-promoting H_2O_2 signalling that is further regulated by peroxiredoxin-3 (PRDX-3). Increased H_2O_2 release in the cytoplasm activates the p38 MAPK signalling cascade that induces KLF-1 translocation to the nucleus and the activation of transcription of *C. elegans* longevity-promoting genes, including cytoprotective cytochrome P450 oxidases. Taken together, our results underline the importance of redox-regulated signalling as the key regulator of longevity-inducing pathways in *C. elegans*, and position precisely timed mitochondria-derived H_2O_2 in the middle of it.

1. Introduction

A limited number of genetic manipulations and treatments warrant increased longevity in multiple species ranging from yeast to higher mammals. Despite very different origins of these manipulations, they all seem to activate longevity assurance pathways that ultimately lead to increased resistance to various stresses, either by switching to alternative metabolic programs or by stimulating cytoprotective machineries [1,2]. The concept that increased resilience leads to increased longevity is not new, still, molecular mechanisms underlying the regulation of stress resistance during ageing are poorly understood.

One of the interventions that extend lifespan is moderate mitochondrial dysfunction, initially shown to be beneficial in the roundworm *C. elegans*, and further confirmed in a wide range of species [3–6]. How can disruption of the mitochondrial electron transport chain (ETC) cause lifespan extension in *C. elegans*, whereas in humans, many mutations that compromise mitochondrial function lead to a variety of pathological, life-shortening diseases? To this end, several different explanations have been proposed. The decreased reactive oxygen species (ROS) production resulting in less oxidative damage due to a lower rate of respiration was initially favoured as the main cause for increased longevity in the *C. elegans* mitochondrial mutants [7,8]. Results from numerous studies in multiple species on the relationship between ROS and ageing in long-lived mutants, mutants with altered mitochondrial function or decreased antioxidant defence, animals treated with antioxidant compounds, and models exposed to different environmental conditions, do not support a straight-forward view that oxidative stress and oxidative damage are the primary cause of ageing (reviewed in Ref. [9]). In fact, ROS, particularly hydrogen peroxide (H_2O_2), are no longer viewed just as a toxic by-product of mitochondrial respiration, but are appreciated for their role in regulating a myriad of cellular signalling pathways, including longevity [10]. Increased H_2O_2 production has been detected in a number of long-lived *C. elegans* mitochondrial mutants leading to the hypothesis that ROS might actually work as a lifespan-promoting signal, which transduces inputs from the mitochondria to other compartments of the cell, resulting in the activation of the longevity-assurance stress responses [11,12]. This adaptive response was named mitochondrial hormesis or mitohormesis [13]. Consistent

* Corresponding author. CECAD Research CenterUniversity of Cologne, Joseph-Stelzmann-Str. 26, Cologne, D-50931, Germany.
E-mail address: aleksandra.trifunovic@uk-koeln.de (A. Trifunovic).

https://doi.org/10.1016/j.redox.2022.102533
Received 31 October 2022; Accepted 7 November 2022
Available online 19 November 2022

with this, mild treatment with paraquat, a chemical compound known to induce H_2O_2 production, and antimycin a, a CIII blocker known to increase mitochondrial superoxide ($O_2^{\bullet -}$) generation, extends the life span of wild-type (N2) *C. elegans* animals [8,11]. However, molecular mechanisms and signalling steps that allow cells to respond to low versus high oxidative stress are largely unknown.

We recently identified Krüppel-like factor 1 (KLF-1) as a mediator of a cytoprotective response that dictates longevity induced by reduced mitochondrial function in long-lived *C. elegans* mitochondrial mutant *isp-1(qm150);ctb-1(qm189)* [14]. This mutant carries mutations in genes encoding two mitochondrial respiratory complex III subunits, nucleus-encoded Rieske protein (ISP-1) and mtDNA-encoded cytochrome *b* (CTB-1) [6]. Our data showed that KLF-1 is essential for the longevity of *isp-1(qm150);ctb-1(qm189)* worms, as without it the lifespan of mutant worms would not differ from wild-type. Remarkably, KLF-1 absence did not affect lifespan in control (N2) animals, making it a true transcriptional regulator of stress-induced hormetic response [14]. A redox-regulated KLF-1 activation and transfer to the nucleus coincide with the peak of somatic mitochondrial biogenesis and aerobic respiration in worms, both of which occur around a transition from the third larval stage (L3) to day-one-of-adulthood (D1) [14–16]. Remarkably, downregulation of mitochondrial function only during this period is sufficient to prolong the lifespan [17]. Therefore, we propose that these 18–20 h during late larval development serve as an important checkpoint for mitochondrial function that is vital for lifespan regulation [14]. We further showed that KLF-1 activates genes involved in the Phase I xenobiotic detoxification program and identified cytochrome P450 oxidases (CYPs), as the main KLF-1 effectors [14]. Like KLF-1, we found that CYPs are essential for the increased longevity of *isp-1(qm150);ctb-1(qm189)* mutants [14]. These findings underline the importance of xenobiotic detoxification in the mitohormetic, longevity-assurance pathway and identify redox signalling cascade in *C. elegans* and KLF-1

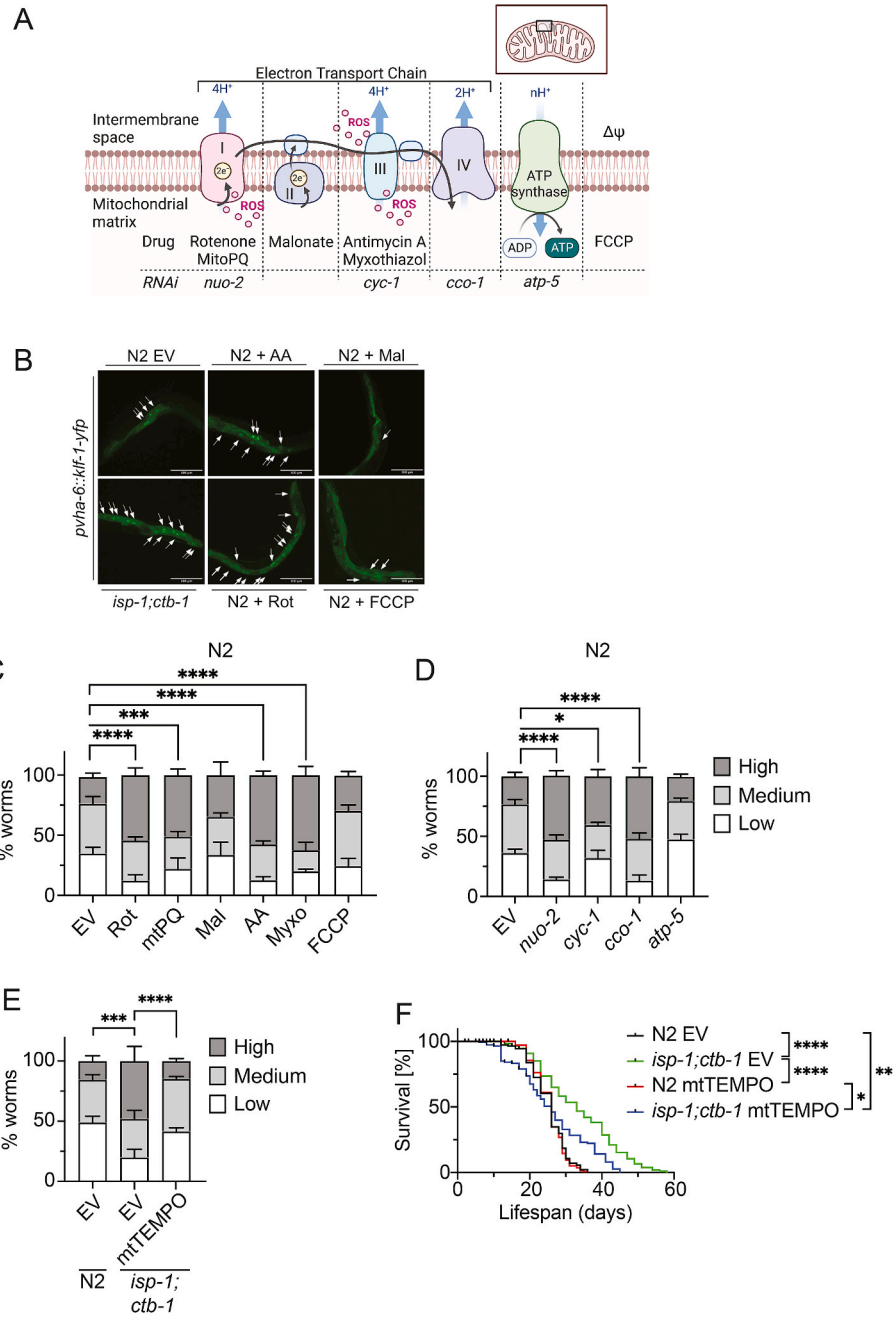

Fig. 1. Mitochondrial-produced ROS activates KLF-1 nuclear localization. A) Schematic representation of the mitochondrial ETC and the sites of inhibition, either via drug or RNAi treatment. B) Representative images of KLF-1-YFP, expressed under gut-specific *vha-6* promoter. Arrows indicate YFP-positive gut nuclei. C-E) D1 animals were assayed based on KLF-1-YFP-positive nuclear localization as followed: 'low' as less than 2 nuclei, 'medium' as 3–6 nuclei, and 'high' as more than 6 nuclei. Data are presented as mean ± SEM. $^{*}p < 0.05$, $^{***}p < 0.001$, $^{****}p < 0.0001$, Chi-square test. n=30 animals per condition. C) N2 animals were grown on control plates and on L4 stage transferred to plates containing 100 nM rotenone (Rot), 5 μM mitoparaquat (mtPQ), 25 mM malonate (Mal), 2 μM antimycin a (AA), 10 μM myxothiazol (Myxo) or 5 μM FCCP. E-F) N2 and *isp-1;ctb-1* animals upon 300 μM mtTEMPO from L3 until D1. F) Lifespan assays. n = 200 animals per condition.

as central factors orchestrating this response.

Here we describe a signalling cascade leading to the activation of KLF-1 in worms and its translocation to the nucleus. We identified antioxidant enzymes that are needed for the regulation of mitochondrial H_2O_2 in *C. elegans*, which is then released into the cytosol by porin/VDAC-1 transporter. This increased H_2O_2 pulse changes the cytosolic redox state in D1 *isp-1;ctb-1* worms and leads to the activation of stress-induced p38 MAPK signalling cascade that ultimately leads to the translocation of KLF-1 to the nucleus and activation of mitohormetic response.

2. Results

2.1. Mitochondrial ROS activates KLF-1-mediated longevity

To further elucidate the role of KLF-1 activation in the longevity assurance of *C. elegans* mitochondrial mutants, we analysed KLF-1 nuclear localization upon various conditions that induce mitochondrial dysfunction, using previously developed reporter strain with KLF-1 tagged to a yellow fluorescent protein (YFP), under the control of gut promoter *vha-6* (*pvha-6::klf-1-yfp*) [14]. Similar to wild-type controls, worms carrying this reporter respond to paraquat treatment by increasing their lifespan (Fig. S1A). As we previously showed that KLF-1 longevity assurance function is required particularly during early adulthood [14], we focused our studies on D1, unless stated differently.

To monitor the effect of mitochondrial dysfunction we utilized various drugs or RNAi against respiratory chain subunits of different OXPHOS complexes (Fig. 1A). To diminish complex I (CI) activity we used two inhibitors, rotenone which block the transfer of electrons from the iron-sulphur subunits to ubiquinone, and mitoparaquat (MitoPQ), a mitochondrial matrix-targeted redox cycler [18,19]. Treatment with either of these drugs results in incomplete electron transfer and increased $O_2^{\bullet}-$production [18,19]. Complex II (CII) dysfunction was induced by exposing the worms to the competitive succinate dehydrogenase inhibitor malonate [20], while treatment with antimycin a or myxothiazol was used to inhibit CIII function [21,22]. Similar to CI inhibitors, both antimycin a and myxothiazol block the electron transfer flow and induce $O_2^{\bullet}-$production [23,24]. Finally, the role of membrane potential was evaluated by treatment with FCCP, a protonophore that acts as a powerful uncoupler of mitochondrial OXPHOS and therefore decreases the chemiosmotic gradient [25]. In addition to chemical inhibitors of mitochondrial OXPHOS, we used RNAi against subunits of CI (*nuo-2*), CIII (*cyc-1*), CIV(*cco-1*), and CV (*atp-5*), treatments previously shown to induce longevity in *C. elegans* [8].

Remarkably, treatment with either chemical inhibitors of CI and CIII, or RNAi-mediated inhibition of CI, CIII, and CIV subunits caused the KLF-1 accumulation in the nucleus (Fig. 1B–D). This is in agreement with our previous observation that the long-lived mitomutant *isp-1;ctb*-1 has elevated levels of nuclear KLF-1, which are essential for lifespan prolongation, without affecting oxygen consumption rates [14]. Here, we could further show that KLF-1 depletion does not affect mitochondrial biogenesis, although some changes in the levels of mitochondrial proteins in *isp-1;ctb-1* mutants were detected (Fig. S1B). The observed KLF-1 translocation to the nucleus and resulting extended lifespan could be prevented by the addition of mitochondria-targeted antioxidant mtTEMPO and vitamin C (Fig. 1E–F, S1C). This is further supported by the finding that treatment with either CII inhibitor malonate or the uncoupler FCCP does not have an effect on the KLF-1 translocation in control worms (Fig. 1B–C). Likewise, an increase in peroxisomal hydrogen peroxide (H_2O_2) levels, through suppression of catalases [26], or higher levels of endoplasmic reticulum (ER)-produced H_2O_2, upon tunicamycin treatment, or ER-stress without increased H_2O_2 production (thapsigargin treatment) [27], largely failed to induce KLF-1 translocation to the nucleus (Fig. S1D). The exception was the down-regulation of catalase 1 (CTL-1) which resulted in the increased KLF-1 nuclear-localization, but failed to increase the longevity in N2 worms arguing that this treatment does not activate KLF-1 signalling pathway in the same way as observed in long-lived *isp-1;ctb-1* mutant (Fig. S1E). Together, these findings highlight mitochondrial ROS as the primary signal in the activation of KLF-1 longevity assurance program.

KLF-1 was shown to be controlled by the HECT ubiquitin E3 ligase WWP-1, a regulator of dietary restriction-induced lifespan [28,29]. The mammalian WWP1 targets different KLFs for proteasome-dependent degradation by polyubiquitylation [30,31]. Conversely, the *C. elegans* homologue, WWP-1 was proposed to regulate KLF-1 function by poly-monoubiquitylation, rather than priming it for degradation, although the mechanism is still unclear [29]. Hence, we next asked if WWP-1 plays a role in mitochondrial dysfunction-induced longevity. Indeed, depletion of WWP-1 in worms increased KLF-1 translocation to the nucleus (Fig. 2A). Unlike in *isp-1;ctb-1* mutant, treatment with vitamin C or NAC only mildly decreased KLF-1 activation upon WWP-1 depletion, but was unable to bring it back to the wild type level (Fig. 2A). Remarkably, the proteasomal inhibition with bortezomib diminished the KLF-1 localization within the nucleus in control worms but did not have much of an effect upon *wwp-1* knockdown, arguing that WWP-1 has a role in the proteasome-mediated KLF-1 degradation (Fig. S2A). The efficiency of proteasomal inhibition was tested using *in vivo* degradation assay and a strain expressing a non-cleavable ubiquitin, N-terminally

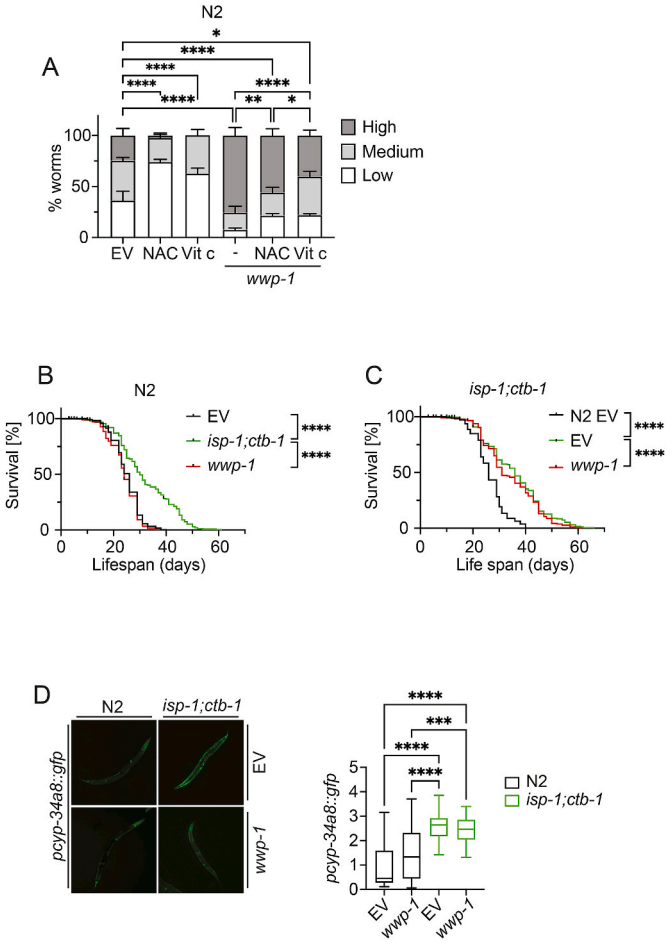

Fig. 2. KLF-1 nuclear translocation is mediated by E3 ligase WWP-1 but is insufficient to induce the longevity-assurance pathway. A) Quantification of KLF-1 nuclear localization in D1 N2 animals upon *wwp-1* RNAi in combination with 10 mM NAC or 10 mM vitamin C (Vit C). Chi-square test. B–C) Lifespan assays. n = 300 animals per condition. B) N2 animals upon *wwp-1* RNAi. C) *isp-1;ctb-1* mutant upon *wwp-1* RNAi. D) Representative pictures and quantification of *pcyp-34a8::gfp* intensity in D1 N2 and *isp-1;ctb-1* worms. n = 20 per condition. Data are presented as mean ± SEM. *$p < 0.05$, **$p < 0.01$, ***$p < 0.001$, ****$p < 0.0001$. D) one-way ANOVA with Tukey post hoc test.

fused to GFP (*psur-5::UbV-GFP*) [32]. We could detect a clear difference in the level of GFP between animals treated with bortezomib or not, confirming the proteasomal inhibition (Fig. S2B).

Next, we wondered if WWP-1 depletion induces longevity in *C. elegans*. Surprisingly, the nuclear accumulation of KLF-1, induced by *wwp-1* RNAi, did not affect the longevity of control (N2) or *isp-1;ctb-1* mutant worms (Fig. 2B–C). To assess if KLF-1 nuclear translocation stimulated by depletion of WWP-1 leads to activation of longevity-assurance pathways and changes we previously described in *isp-1;ctb-1* mutants, we analysed the expression of cytochrome P450 (*cyps*) genes [14]. Curiously, the increased cytoprotective response mediated by high expression of *cyps* was absent upon WWP-1 depletion (Fig. 2D and S2C). In summary, our data establish that WWP-1 regulates subcellular localization of KLF-1, but does not activate longevity-assurance pathways previously described in *isp-1;ctb-1* mutant worms [14], possibly because redox signalling plays only a minor role in the WWP-1 mediated regulation of KLF-1.

2.2. Mitochondrial H_2O_2 production and cytosolic release are essential for the KLF-1 activation

We previously established that mitochondrial OXPHOS dysfunction and redox signalling are the main activators of KLF-1-induced longevity in *C. elegans* [14]. Here, we established that mitochondria-derived ROS is needed for the KLF-1 translocation to the nucleus. Next, we aimed to identify which type of reactive oxygen molecule is able to activate the signalling cascade that connects mitochondrial dysfunction and translocation of KLF-1. While dysfunctional mitochondria primarily produce $O_2^{\bullet}{}^-$, H_2O_2 has been described as the most stable long-lived ROS molecule allowing it to serve as a potential second messenger [33–35]. Certainly, we could show that treatment with exogenous H_2O_2 was sufficient to translocate KLF-1 to the nucleus (Fig. 3A). To identify the redox machinery that modulates the H_2O_2 signalling cascade in *isp-1;ctb-1* mutant worms, we performed an RNAi screen targeting specifically redox enzymes responsible for mediating different steps of H_2O_2 metabolism, by assessing the KLF-1 localization in N2 animals exposed to

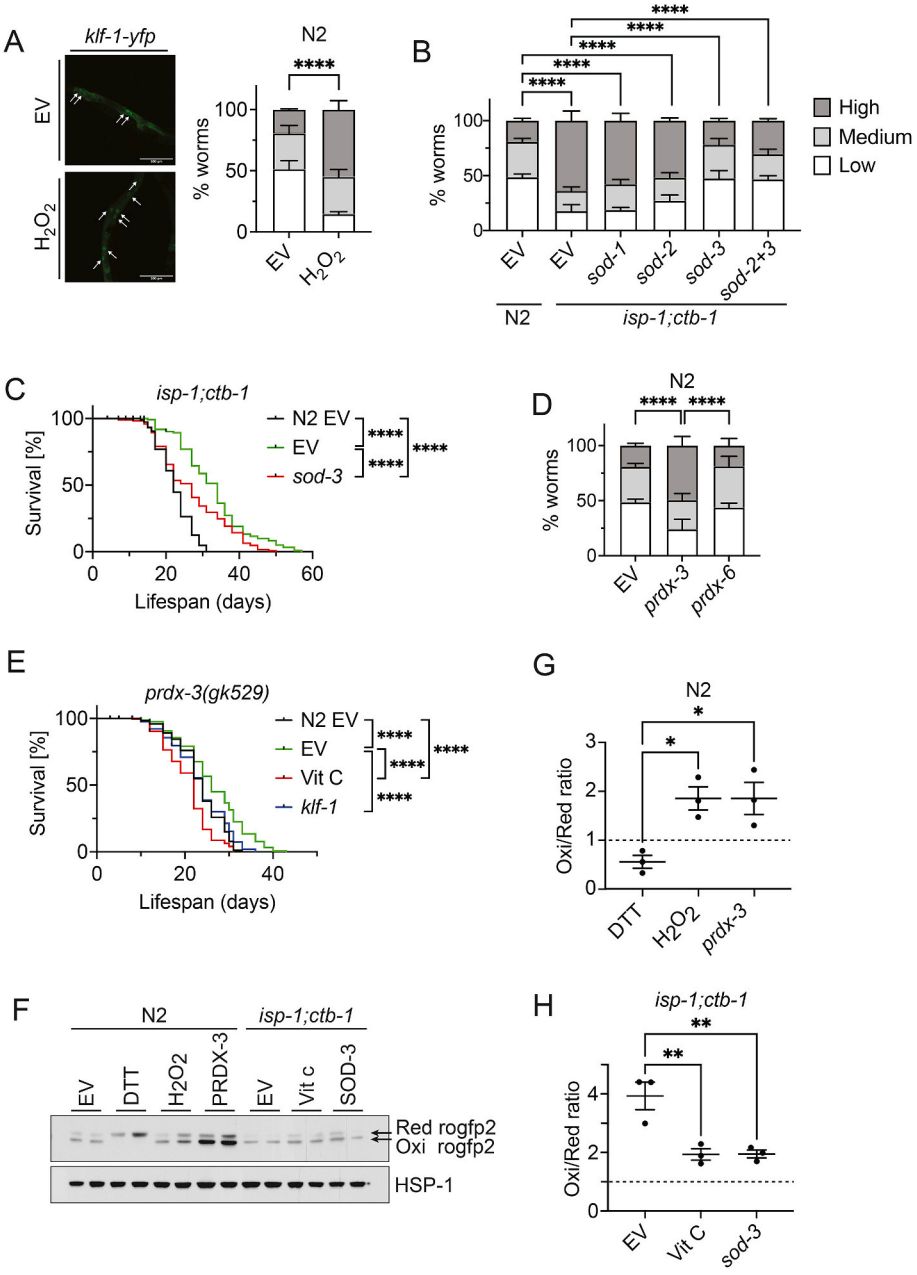

Fig. 3. Mitochondrial H_2O_2 levels are regulated by SOD-3 and PRDX-3. A, B, D) Number of KLF-1-positive nuclei was assayed at D1. n = 30 animals per condition. ****$p < 0.0001$, Chi-square test. A) Representative pictures and quantification of N2 animals upon 30 min of 10 mM H_2O_2 treatment. B) *isp-1;ctb-1* animals upon *sod-1*, *sod-2*, *sod-3* or combined *sod-2* and *sod-3* RNAi. C) Lifespan of *isp-1;ctb-1* mutant upon *sod-3* RNAi. D) N2 animals upon *prdx-3* and *prdx-6* RNAi. E) Lifespan of *prdx-3(gk529)* mutant upon vitamin C or *klf-1* RNAi. C-E) n = 200 worms per condition. F) Immunoblot of whole worm lysates of L4 N2 and *isp-1;ctb-1* animals expressing *pvha-6::tomm-20::roGFP2-Orp1*. The used antibodies were anti-GFP and anti-HSP-1 (loading control). N2 animals were treated with 5 mM dithiothreitol (DTT), 10 mM H_2O_2, or *prdx-3* RNAi. *isp-1;ctb-1* animals were treated with 10 mM vitamin C or *sod-3* RNAi. G-H) Quantification of ratio between oxidized versus reduced roGFP2 and normalized on HSP-1. Data are relative to N2 EV (dashed line). n = 3 per condition. Data are presented as mean ± SEM. *$p < 0.05$, **$p < 0.01$, one-way ANOVA with Tukey post hoc test. G) N2 animals. H) *isp-1;ctb-1* animals.

antimycin a. Out of 22 assayed genes (Table S1), two showed a clear effect on the KLF-1 localization patterns: superoxide dismutase 3 (SOD-3) and peroxiredoxin 3 (PRDX-3).

Superoxide dismutases (SODs) are major antioxidant enzymes that catalyse the dismutation of superoxide anions to hydrogen peroxide [36]. Although *C. elegans* possesses five different SODs, here we focused on the cytosolic/mitochondrial SOD-1 and mitochondrial SOD-2 and SOD-3; as SOD-4 and SOD-5 are present in the extracellular space or in a specific subset of neurons, respectively [37,38]. Remarkably, only SOD-3 depletion in *isp-1;ctb-1* mutant, regardless of the presence of other mitochondrial matrix SOD (SOD-2), fully prevented KLF-1 translocation to the nucleus, while the absence of the other two enzymes (SOD-1 and -2) had no effect (Fig. 3B). We could further show that SOD-3 depletion caused a significant decrease in the longevity of *isp-1;ctb-1* mutant worms (Fig. 3C), while having no effect on N2 lifespan (Fig. S3A). In agreement with previous results that ROS pulse is required during larval development, depletion of SOD-3 only during this period was sufficient to reduce the longevity in *isp-1;ctb-1* mutants (Fig. S3B). Collectively, these results establish H_2O_2 as the main signalling molecule needed for KLF-1 translocation and the activation of longevity-assurance pathway in *C. elegans*, and identify SOD-3 as the key regulator of H_2O_2 biosynthesis in the *isp-1;ctb-1* mutant.

PRDX-3 is a mitochondrial antioxidant enzyme, a member of the thioredoxin peroxidase family that scavenges H_2O_2 [39]. We detected higher KLF-1 translocation to the nucleus upon *prdx-3* RNAi in N2 worms, but not *prdx-6*, predicted to be mainly cytosolic, translocating to mitochondria only upon stress [40], in agreement with the expected increase in H_2O_2 levels (Fig. 3D). Furthermore, we show that *prdx-3 (gk529)* mutants [41] are long-lived compared to control animals (Fig. 3E). In contrast, cytosolic *prdx-2(gk169)* mutant [42] have shorter lifespan (Fig. S3C). The longevity of *prdx-3(gk529)* mutants could be prevented by both KLF-1 depletion and treatment with vitamin C (Fig. 3E), indicating involvement in the redox-regulated, KLF-1-mediated, longevity-assurance pathway in *C. elegans*. In agreement, DTT, a reducing agent that prevents disulphide bond formation, strongly reduced the level of KLF-1 in the nucleus in both N2 and *isp-1;ctb-1* animals, whereas diamide, a thiol oxidant that induces disulphide bond formation, elated the level of KLF-1 in nucleus in N2 (Fig. S3D).

Next, we wanted to determine if H_2O_2 acts directly as a secondary messenger that activates KLF-1 translocation in *C. elegans*, hence is released from the mitochondria into the cytosol. We used a pH-independent H_2O_2 sensor roGFP2-Orp1, which is a combination of a redox-sensitive GFP variant (roGFP2) fused to the H_2O_2 sensing yeast peroxidase Orp1 (Gpx3), previously shown to work well in different organisms [43–45]. To visualize the H_2O_2 levels just outside of the mitochondria, we used the roGFP2-Orp1 tagged to the N-terminal part of TOMM-20 (mitochondrial import receptor subunit TOM20 homologue), which is embedded in the outer mitochondrial membrane, facing outwards [46]. The measurements were performed at larval stage 4 (L4) which we previously identified as a major time point for mitochondrial biogenesis and ROS burst needed to activate KLF-1 – mediated longevity assurance program [14,15]. To validate the roGFP2-Orp1 sensor in our setting, we treated the control N2 worms expressing roGFP2-Orp1 in the body wall muscle with either H_2O_2 to increase oxidized roGFP2 levels, or with DTT to decrease them (Fig. S3E). As expected, we could observe an increase in oxidized roGFP levels upon treatment with H_2O_2, but not in control conditions or after DDT addition (Fig. S3F). Next, we assessed the H_2O_2 release in the *C. elegans* gut, the main site of the *klf-1* expression, using immunoblotting to estimate the levels of reduced and oxidized roGFP2 (Fig. 3F and S3G), as an imaging-based approach was unfeasible due to high bacterial autofluorescence. As previously shown in the body wall muscle, higher levels of oxidized roGFP at the outer mitochondrial membrane (OMM) were detected upon treatment of N2 worms with H_2O_2 or *prdx-3* RNAi, while DTT treatment had the opposing effect (Fig. 3G). Correspondingly, *isp-1;ctb-1* mutant worms showed high levels of oxidized TOMM-20:roGFP2, suggesting higher release of mitochondrial H_2O_2 into the cytoplasm, that was largely prevented by the treatment with vitamin C or *sod-3* RNAi (Fig. 3H). This was independent of the glutathione levels that were consistently lower in *isp-1;ctb-1* worms, while the GSH/GSSG ratio was similar to control N2 animals (Fig. S3H).

To understand the cytosolic part of the signalling cascade that activates KLF-1, we investigated the effect of increased mitochondrial H_2O_2 release on the cytosolic redox state using Grx1-roGFP2 sensor [47]. Remarkably, when the cytosolic redox state was analysed in L4 animals, a trend toward increase, but no significant difference was observed between N2 and *isp-1;ctb-1* worms (Fig. 4A and S4A). Still, only a day later, on D1, we could detect a strong increase in the oxidized cytosolic roGFP2 sensor *isp-1;ctb-1* mutant, while levels in N2 control animals remained unchanged (Fig. 4A and S4A). Therefore, these data provide clear evidence for the timed H_2O_2 release from mitochondria to the cytoplasm in *isp-1;ctb-1* worms that coincide with the KLF-1 activation and translocation to the nucleus.

As the diffusion of H_2O_2 across membranes is limited, facilitated transport is typically required [48]. Therefore, we asked which channel might be responsible for the H_2O_2 transport across mitochondrial membranes in *C. elegans*? Previously, it was suggested that aquaporins and VDAC might play a vital role in H_2O_2 transport outside of mitochondria [48–50]. Therefore, we performed a targeted RNAi screen on *isp-1;ctb-1* worms by depleting aquaporins (*aqp-1* to *aqp-12*) and *vdac-1*, the only voltage channel present in *C. elegans* mitochondria [51,52]. Whereas the RNAi against different *aqp* genes showed no alteration in the number of KLF-1-positive nuclei, VDAC-1 depletion resulted in a strong decrease of KLF-1 nuclear translocation (Fig. 4B). We further showed that VDAC-1 depletion reduces the longevity of *isp-1;ctb-1* animals, whereas it does not have an effect on N2 lifespan (Fig. 4C and S4B, respectively). Similar to SOD-3 depletion, loss of VDAC-1 only during larval development is sufficient to reduce the *isp-1;ctb-1* lifespan (Fig. S4C). Further supporting the role of VDAC-1 in the H_2O_2 export from mitochondria, its loss significantly decreased the level of oxidized TOMM-20:roGFP2 in *isp-1;ctb-1* animals (Fig. 4D). These findings illustrate the key roles of SOD-3, PRDX-3, and VDAC-1 in mitochondrial H_2O_2 signalling, and KLF-1-activation and translocation to the nucleus in *C. elegans* (Fig. 4E).

To address the role of the observed mitochondrial signalling cascade in activating the KLF-1-dependent cytoprotective machinery, we analysed the cytosolic GRX1-roGFP2 sensor and the expression levels of *cyp-34a8* [14]. Compatible with the notion that mitochondrial H_2O_2 is required for the activation of KLF-1, N2 animals upon *prdx-3* RNAi demonstrated an increased oxidized/reducted Grx1-roGFP2 ratio, whereas antioxidant treatments or *sod-3* or *vdac-1* RNAi decreased this ratio in *isp-1;ctb-1* animals (Fig. 5A). Upon WWP-1 depletion the ratio was unaltered in N2 animals (Fig. 5A). Similarly, an increase in the *cyp-34a8* level was observed in N2 animals upon PRDX-3 depletion (Fig. 5B). Correspondingly, high levels of *cyp-34a8* observed in *isp-1;ctb-1* were decreased upon *sod-3* or *vdac-1* RNAi (Fig. 5B). We previously showed that higher levels of different CYPs give a survival advantage upon contact with xenobiotics [14]. To validate this here, we either assayed the resistance to levamisole-induced paralysis or followed the development of worms in the presence of vinblastine, a compound that prevents cell proliferation and is cleared by action of CYPs (Fig. 5C–F). In the conditions that result in higher H_2O_2 levels, like upon *prdx-3* RNAi or in *isp-1;ctb-1* mutants, we detected better levamisole-induced paralysis resistance (Fig. 5C, E), and worms reached further stages in development when exposed to vinblastine (Fig. 5D, F). In contrast, when *isp-1;ctb-1* mutants were exposed to treatments that should decrease H_2O_2 levels, like grown in the presence of vitamin C, *sod-3* or, *vdac-1* RNAi, they were less resistant to levamisole-induced paralysis and had slower development on vinblastine, largely matching that of N2 worms (Fig. 5D–E, S5A). This is even more striking considering that normally, *isp-1;ctb-1* mutants show a strong delay in larval development compared to N2 controls [6].

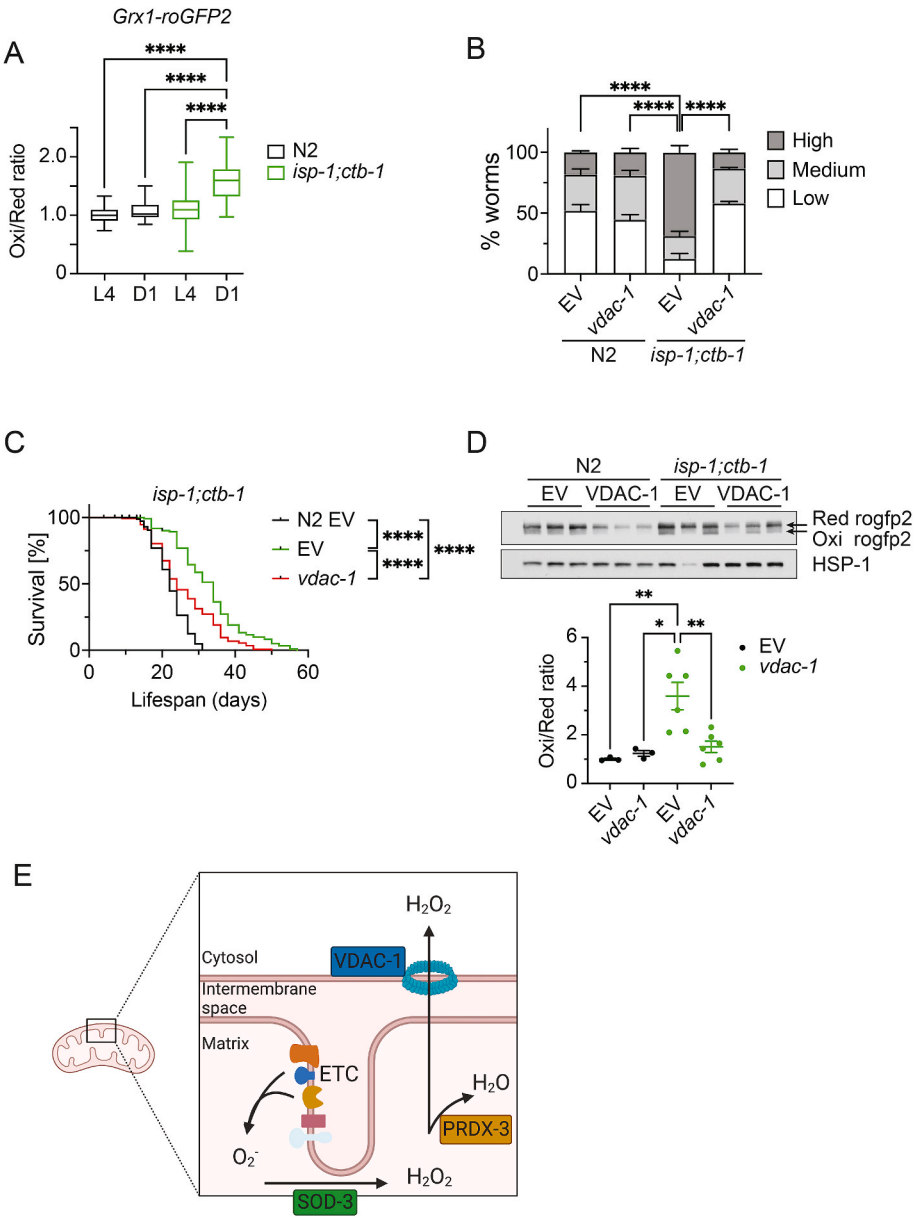

Fig. 4. VDAC-1-dependent mitochondrial H_2O_2 release increases the cytoplasmic oxidation state. A) N2 and *isp-1;ctb-1* animals expressing *Grx1-roGFP2*. Data shown is the ratio between oxidized versus reduced $roGFP_2$ and normalized on N2 L4. n = 25 animals per condition. $^{****}p < 0.0001$, one-way ANOVA with Tukey post hoc test. B) Quantification of KLF-1 nuclear localization in N2 and *isp-1;ctb-1* worms upon *vdac-1* RNAi. n = 30 animals per condition. $^{****}p < 0.0001$, Chi-square test. C) *isp-1;ctb-1* lifespan on *vdac-1* RNAi. n = 200 worms per condition. D) Quantification of immunoblot of whole worm lysate of L4 N2 and *isp-1;ctb-1* animals expressing *pvha-6::tomm20::roGFP2-Orp1*. Anti-GFP and anti-HSP-1 (loading control) antibodies were used. Shown is the ratio between oxidized versus reduced roGFP2 corrected for HSP-1 and data are normalized on N2 EV. n = 3 per condition. Data are presented as mean ± SEM. $^{*}p < 0.05$, $^{**}p < 0.01$, one-way ANOVA with Tukey post hoc test. E) Schematic pathway demonstrating our findings.

2.3. *Oxidized cytosolic redox state activates KLF-1 nuclear localization via p38 MAPK signalling*

Repositioning of transcriptional factors between cytoplasm and nucleus is often regulated by signals relying on altering nuclear localization (NLS) and nuclear export signal (NES). Like some mammalian KLFs, nematode KLF-1 is predicted (cNLS Mapper [53]) to have NLS in a cluster of basic amino acids immediately preceding the first zinc finger [54,55]. The predicted NLS has positively charged lysine (K), anticipated to strongly binds to importin (Fig. S6A) [56]. To test if this conserved amino acid residue is required for the nuclear KLF-1 translocation, we mutated positively charged lysine into neutral alanine (K411 > A). Our results demonstrated that K411 is indeed necessary for the KLF-1 nuclear translocation upon either addition of H_2O_2 or *wwp-1* RNAi-mediated depletion (Fig. 6A, S6B). The loss of lysine (K411 > A) strongly diminished the KLF-1 nuclear translocation, although some level of induction could be observed in treated K411 > A worms (H_2O_2 or *wwp-1* RNAi) when compared to untreated controls (Fig. 6A, S6B). The overexpressed K411 > A KLF-1 variant also decreased lifespan of control worms and further prevented longevity induction upon treatment with paraquat (Fig. S6C), in agreement with the role of KLF-1 nuclear localization in the redox-regulated longevity-assurance.

The differences between KLF-1 nuclear localization and lifespan extension, such as in the case of *wwp-1* knockdown, suggest the existence of a second level of KLF-1 regulation in *isp-1;ctb-1 C. elegans* mutants. To further elucidate the upstream components in the KLF-1 activation cascade in the cytoplasm in *isp-1;ctb-1* animals, we used two approaches. First, we screened for the kinases and phosphatases that regulate KLF-1 translocation upon mitochondrial dysfunction. We turned to kinases and phosphatases as they are the prototypic targets used to apprehend the fine-tuning of redox-modification in the regulation of phosphorylation-driven signalling cascades [57]. Making use of an available *C. elegans* database that predicts over 600 kinases and phosphatases (www.kinase.com, Salk Institute, CA, USA), we performed a targeted RNAi screen using D1 old worms exposed to low concentrations of antimycin a, that induces strong KLF-1 nuclear localization (Fig. 1C). Depletion of only a handful of kinases/phosphatases prevented KLF-1 translocation in the conditions of increased mitochondrial dysfunction and H_2O_2 production in *C. elegans* (Table S2). Among these, PMK-3 and NSY-1 caught our attention as they are part of the p38 MAPK (mitogen-activated protein

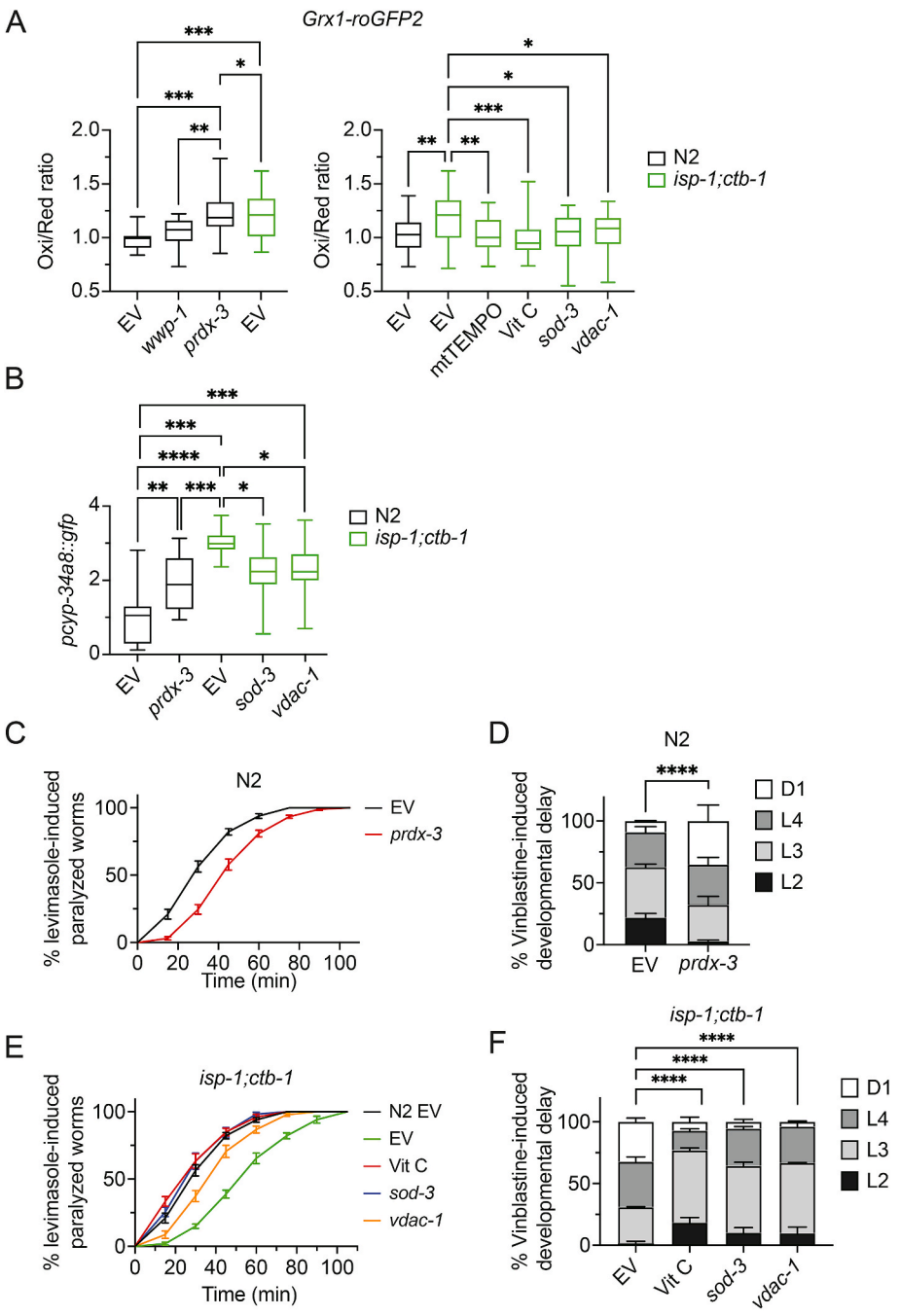

Fig. 5. Mitochondrial H_2O_2 signalling pathway regulates Phase I detoxification. A) N2 (left) and *isp-1; ctb-1* (right) animals expressing *Grx1-roGFP2*. Data shown is the ratio between oxidized versus reduced $roGFP_2$. B) Expression levels of *pcyp-34a-8::gfp* in N2 and *isp-1;ctb-1* animals upon *prdx-3*, *sod-3* or *vdac-1* RNAi. n = 20 animals per condition. A, B) Data were normalized to N2 EV and are presented as mean ± SEM. *$p < 0.05$, **$p < 0.01$, ***$p < 0.001$, ****$p <$ 0.0001, one-way ANOVA with Tukey post hoc test. C, D) N2 animals upon *prdx-3* RNAi. E, F) *isp-1;ctb-1* animals upon vitamin C and *sod-3* and *vdac-1* RNAi. C, E) Worms were transferred on the fourth day of adulthood on plates containing 1 mM of levamisole. Animals were assayed every 15 min for movement. Failure to move was regarded as paralysed. N = 80 animals per condition. D, F) L1 animals were grown in liquid with or without 100 μM vinblastine. When untreated vinblastine animals reached first day of adulthood, the conditions with vinblastine treatment were scored for developmental stages. n = 200 animals per condition. Data are presented as mean ± SEM. ****$p < 0.0001$, Chi-square test.

kinase) signalling cascade shown to be stimulated by the fluctuation of the cellular redox state (Fig. S7A) [58–61]. Remarkably, through analysis of KLF-1 interacting partners using a co-immunoprecipitation (Co-IP) of FLAG-tagged KLF-1 from N2 and *isp-1;ctb-1* animals, followed by mass spectrometry, we identified SEK-1, the third kinase in the p38 MAPK signalling pathway (Fig. S7A and Table S3). First, we could show that PMK phosphorylation is increased in *isp-1;ctb-1* mutant on D1, but not in L4 stage, in agreement with our previous results that cytoplasmic redox environment is changed only on D1 (Fig. 6B). Furthermore, treatment with SB203580, an inhibitor of p38 mitogen-activated protein kinases, including PMKs was able to prevent the KLF-1 translocation to the nucleus and subsequent activation of *cyp-34a8* expression (Fig. 6C–D, S7B). Undesirably, pull-downs coupled with mass spectrometry or Western blot using antibodies against phosphorylated serine and threonine residues failed to detect any signs of direct KLF-1 phosphorylation in *isp-1;ctb-1* mutant (Fig. S7C).

We then proceeded to further analyse the role of all MAPK kinases in the regulation of KLF-1 stress-induced pathway. Depletion of either of these proteins (NSY-1, SEK-1, and PMK 1–3) resulted in a strongly decreased KLF-1 translocation in *isp-1;ctb-1* mutant worms (Fig. 6E). A similar effect was observed in control N2 animals, where RNAi against *nsy-1*, *sek-1,* and *pmk-3* led to a moderated decrease in KLF-1 nuclear localization (Fig. S7D). Remarkably, depletion of either of the PMKs resulted in the reduction of *isp-1;ctb-1* lifespan mutants (Fig. 6F), while *pmk-1* and *pmk-2* RNAi also shortened lifespan of N2 animals (Fig. S7E). Despite a similar effect on lifespan, only PMK-3 seems to be involved in the specific activation of KLF-1 mediated longevity-assurance program in *C. elegans*, as only *pmk-3* RNAi was able to consistently and strongly diminish the expression of different *cyps* to levels similar to a decrease observed when KLF-1 is depleted (Fig. 6G and S7F-G). In summary, these

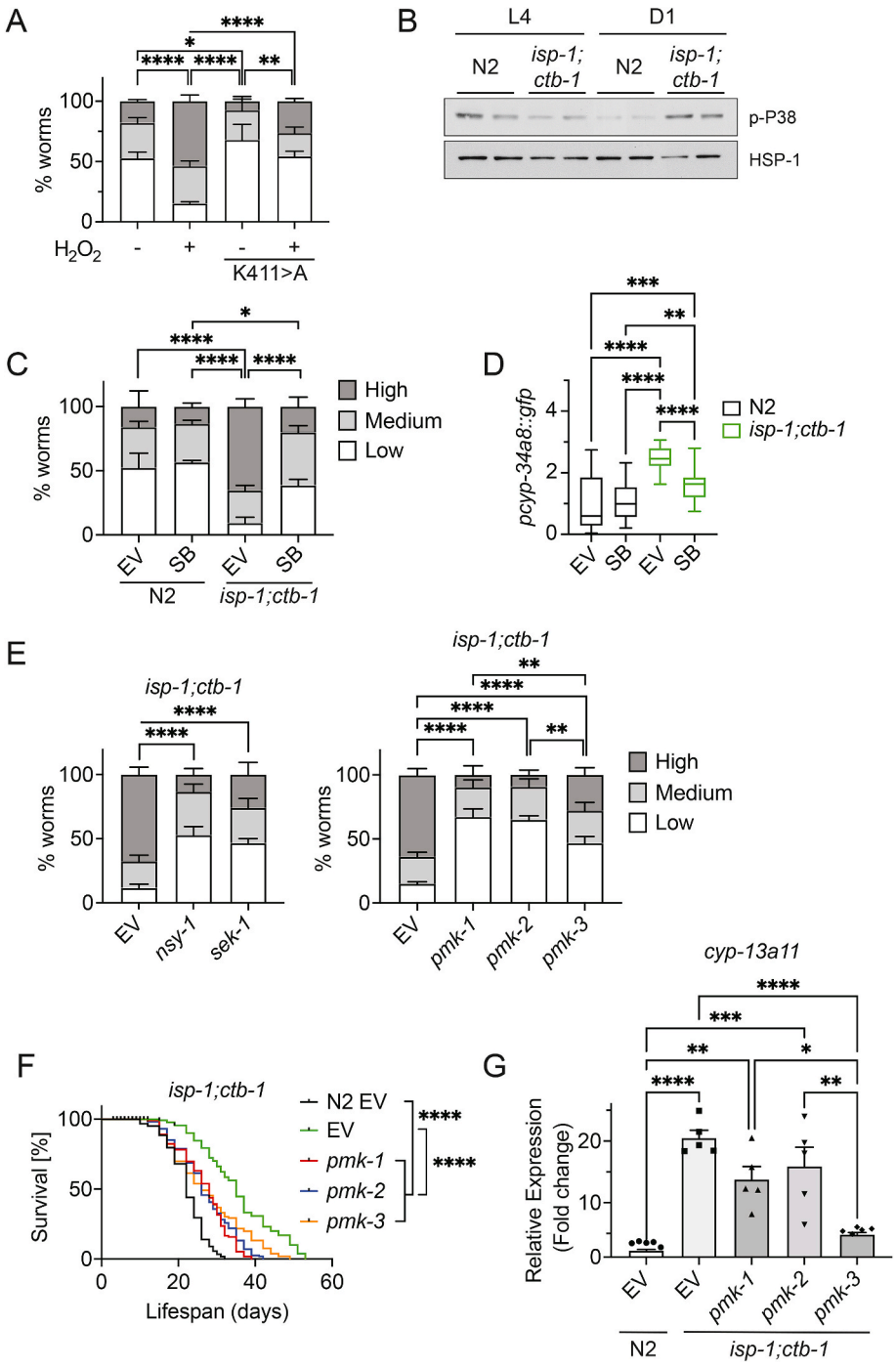

Fig. 6. Increased oxidized cytosolic redox state activates p38 MAPK pathway. A, C, E) Quantification of KLF-1-positive nuclei in D1 animals. n = 30 animals per condition. Data are presented as mean ± SEM. $^{**}p < 0.01$, $^{****}p < 0.0001$, Chi-square test. A) N2 animals expressing *klf-1-yfp* construct with lysine (K) 411 of KLF-1 mutated to alanine. Worms were treated with 10 μM H_2O_2 prior to imaging. B) Western blot from L4 and D1 animals where anti-P-p38 (p-PMK) and anti-HSP-1 (loading control) were used. C-D) Animals treated with p38 inhibitor (SB203580). D) Quantification of *pcyp-34a8::gfp* intensity n = 20 per condition. E) Left) *isp-1;ctb-1* upon *nsy-1* and *sek-1* RNAi. Right) *isp-1;ctb-1* upon *pmk-1*, *pmk-2,* or *pmk-3* RNAi. F) Lifespans of *isp-1;ctb-1* mutant on *pmk-1*, *pmk-2,* or *pmk-3* RNAi. n = 200 animals per condition. G) *cyp-13a11* expression levels were measured by qPCR upon *pmk-1*, *pmk-2*, or *pmk-3* RNAi. n = 4 per condition. Data were normalized to N2 EV and are presented as mean ± SEM. $^{*}p < 0.05$, $^{**}p < 0.01$, $^{***}p < 0.001$, $^{****}p < 0.0001$, one-way ANOVA with Tukey post hoc test.

findings clearly show that p38 MAPK pathway is important for the cytosolic part of the KLF-1 signalling cascade in *C. elegans*.

3. Discussion

Molecular mechanisms regulating longevity-assurance pathways initiated by moderate level of mitochondrial deficiency in *C. elegans* are still poorly understood. Here we identified a signalling cascade driven by mitochondrial H_2O_2 and p38 MAPK pathway, resulting in nuclear translocation of KLF-1 transcription factor and consequently promotion of longevity in *C. elegans* (Fig. 7). We demonstrated that mitochondrial dysfunction as observed in *isp-1;ctb-1* mutant worms, induces production of superoxide anions through defective electron transport chain, leading to increased mitochondrial H_2O_2 levels, in large part mediated by SOD-3. To remove toxic H_2O_2 accumulation, mitochondria rely on detoxification by PRDX-3 and VDAC-1 – mediated H_2O_2 transport to cytoplasm (Fig. 7). Finally, we showed that the expelled mitochondrial H_2O_2 results in a more oxidized redox state in the cytoplasm, leading to the initiation of p38 MAPK signalling cascade, which in turn prompts the KLF-1 activation and translocation to the nucleus. In the nucleus, KLF-1 initiates a mitohormetic stress response by regulating the expression of xenobiotic detoxification genes and promoting lifespan extension in *C. elegans* [14].

Remarkably, we show that E3 ligase WWP-1 can promote KLF-1 translocation to the nucleus without activating the mitohormetic response in *C. elegans*. While we showed that mitochondrial dysfunction-

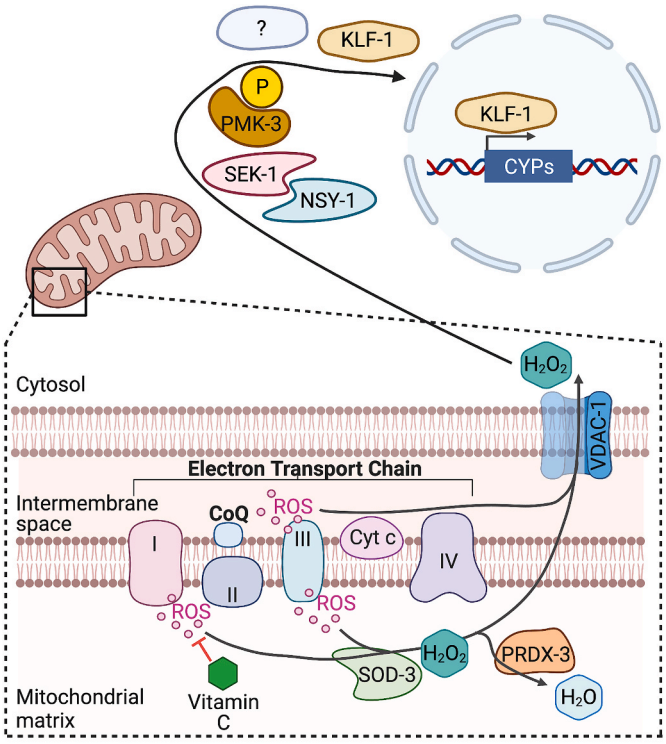

Fig. 7. Mitochondrial H_2O_2 release, dependent on SOD-3, PRDX-3 and VDAC-1 is translocating KLF towards the nucleus, which is mediated by p38 MAPK, especially PMK-3. Schematic overview of the proposed model.

induced longevity is independent of WWP-1, others argued about its involvement in the longevity assurance in both insulin/IGF-1 (IIS) and dietary restriction (DR)-induced pathways in worms [28,62]. The effect of WWP-1 and the proposed poly-monoubiquitination on KLF-1 remains ambiguous although it has been suggested that these modifications might activate and prime nematode's KLF-1 to the nucleus [63]. Our data argue that in *C. elegans* WWP-1 rather acts as a negative regulator of KLF-1 by promoting its degradation, either by inhibiting KLF-1 translocation to the nucleus or by promoting KLF-1 expulsion from the nucleus. Similar roles have been proposed for mammalian WWP1 in the regulation of multiple KLFs [30,31,64]. It was shown that in mammalian cells, WWP1 functions as a cofactor that binds KLF2 thus suppressing the transactivation of target genes [64], while another study argued that the interaction of WWP1 with KLF2 mediates poly-ubiquitination and proteasomal degradation of the later [30]. Similarly, mammalian WWP1 mediates the ubiquitination and degradation of KLF5 through interaction with PY motif in the KLF5 transactivation domain [31]. Remarkably the primary site of the interaction of WWP1 - KLF5 was suggested to be the nucleus, in agreement with our results [31].

We demonstrated that KLF-1 translocation to the nucleus in *C. elegans* can be induced by both chemical inhibition and depletion/dysfunction of CI, CIII, and CIV, and is prevented by the use of antioxidants. This is in agreement with our previous results that KLF-1 is needed for lifespan prolongation in different *C. elegans* mitochondrial mutants [14]. Exposure to low concentration of paraquat (PQ), which favours the generation of ROS at CI can extend the lifespan of N2 worms [11,65,66]. A similar mechanism of lifespan extension was proposed for the *C. elegans* mitochondrial mutants, in part because PQ could not further extend the lifespan of the *isp-1* and *nuo-6* mutants, while it had an additive effect on IIS and DR long-lived mutants (e.g. *eat-2* and *daf-2*) [11]. Various beneficial effects of low levels of H_2O_2 have been described in multiple organisms, and it was proposed that several longevity-promoting interventions cause a mild increase in the mitochondrial ROS formation, hence inducing long-lasting resistance to oxidative stress, a response known as mitohormesis [13,67–69]. In agreement, antioxidant supplements in mammals were shown to interfere with the health- and longevity-promoting abilities of CR and physical exercise [13]. Nevertheless, most of these studies failed to offer mechanistic clarification for the observed phenotypes. In contrast, we provide strong evidence for the involvement of SOD-3, PRDX-3, and VDAC-1 as direct regulators of mitochondrial H_2O_2 signalling cascade in *C. elegans* and KLF-1 activation in the *isp-1;ctb-1* mutant worms. Strongly consistent with our data, a previous study found that SOD-3 was essential for the pro-longevity signal induced by PQ treatment in *C. elegans* [70]. A different study implied that PRDX-3 function might be precisely timed to the larval phases, as *prdx-3* RNAi on adult worms had no effect on lifespan, but decreased oxidative stress resistance [71]. We showed that *prdx-3* RNAi-mediated depletion only during larval stages increases the lifespan, in agreement with our hypothesis that longevity promoting H_2O_2 pulse coincides with the developmental phases where aerobic respiration and somatic mitochondrial biogenesis peak [14,72,73]. Similar regulation has been described for the Yap1 transcription factor that regulates H_2O_2 homeostasis in *Saccharomyces cerevisiae* [74]. Yap1 is activated when H_2O_2 levels increase through its interaction with glutathione peroxidase-like enzyme Gpx3/Orp1 which also serves as sensor and transducer of the H_2O_2 signal to Yap1 [74].

While the metabolism of H_2O_2 in mitochondria is extensively studied, much less is known about the transport of H_2O_2 across mitochondrial membranes. Unlike superoxide, H_2O_2 can slowly diffuse across the inner mitochondrial membrane (IMM), while VDACs in the OMM likely allow for unrestricted diffusion into the cytosol [75]. Correspondingly, overexpression of VDAC-1 in *C. elegans* resulted in animals that were highly sensitive to paraquat treatment and had a strongly decreased lifespans [76]. Even less is known about the transport across IMM, and it is possible that H_2O_2 passage might be facilitated by some aquaporins as described in other cellular membranes [77]. Although we demonstrated that depletion of the known *C. elegans* aquaporins does not affect KLF-1 nuclear-translocation in *isp-1;ctb-1* mutant, we cannot exclude a possibility that they still play a part in the H_2O_2 transport across IMM, but might have redundant roles which our experimental approach could not uncover.

Changes in redox activate a plethora of signalling pathways, with stress-activated p38 MAPK signalling being possibly the most studied and relevant one [78]. In mammals, phosphorylation events were shown to increase the recognition of the NLS by nuclear importers [79,80]. Not surprisingly, p38 MAPK signalling was also described as a regulator of various stress-responsive transcription factors, including DAF-16/FOXO1 and SKN-1/NRF2 which are also implied in the regulation of longevity in different species [78,81,82]. Remarkably, our approaches to identify regulators of KLF-1 translocation in *isp-1;ctb-1* mutant worms led to the identification of the proteins involved in every step of p38 signalling pathway including NSY-1 (MAPKKK), SEK-1 (MAPKK) and PMK-3 (MAPK). Mammalian homologue of NSY-1, ASK1 was described as one of the first proteins relying on oxidative stress-dependent activation [83]. It is therefore likely that increased levels of oxidation as observed in *isp-1;ctb-1* mutant worms lead to the NSY-1/ASK1 activation, which subsequently drives p38 MAPK signalling cascade. In further agreement with our findings, SEK-1 induces a cytoprotective machinery in dietary restriction-mediated longevity, by increasing the nematode's xenobiotic detoxification program [84], while both SEK-1 and SEK-3 were identified in a screen for factors regulating extended the lifespan of *C. elegans* mitochondrial mutants [85]. In the later study, PMK-3 was shown to be a key regulator of longevity in *isp-1(qm150)* and *nuo-6(qm200)* mutant worms, and upon *nuo-2* and *cco-1* RNAi, although no further mechanistic insight was provided [85]. A different p38 homologue, PMK-1 was shown to regulate the activation of SKN-1, a transcription factor that controls Phase II of the xenobiotic detoxification pathway in *C. elegans,* while we showed that Phase I response is controlled by KLF-1 [14,81]. It seems that in *C. elegans*, upon oxidative stress, distinct p38 MAPKs/PMKs may

regulate the activation of different branches of the xenobiotic detoxification response, while the upstream effectors of the MAPK signalling (SEK-1 and NSY-1) are the same [14,81]. This might warrant separate control over the two phases as they have distinctive roles and control different sets of genes [86]. While Phase I primarily encodes cytochrome P450 enzymes, which catalyse the addition of oxygen to form a reactive site on the toxic compound, phase II encompasses conjugation enzymes and antioxidant support systems that add a water-soluble group to this reactive site [86,87]. Therefore, the Phase I and II detoxification enzymes might have a very different schedule in cells under stress, hence the regulation by the same pathway, while having a different final effector sounds plausible.

The most challenging and still open questions arising from our study are: how is KLF-1 activated by the H_2O_2 signalling, and how is specificity of the response achieved independent of KLF-1 nuclear localization? We have shown that p38 MAPK signalling is needed for both KLF-1 translocation to the nucleus, but also lifespan prolongation in *isp-1;ctb-1* mutants and the activation of CYPs, the longevity-assurance genes in *C. elegans*. Sadly, despite multiple efforts, we have not detected proof of direct PMK/p38 MAPK- mediated phosphorylation of KLF-1. Therefore, it is possible that, depending on the redox status of the cell, the p38 MAPK pathway phosphorylates a currently unknown KLF-1 interacting partner, thus ensuring activation of the longevity-inducing xenobiotic-detoxification response, observed in *C. elegans* mitochondrial mutants. As redox status does not seem to change upon depletion of WWP-1, this scenario can also explain the lack of activation of longevity-assurance program upon WWP-1 depletion.

In conclusion, these results identify the redox signalling cascade necessary for longevity assurance in *C. elegans* mitochondrial mutants that depends on mitochondrial H_2O_2 signalling, redox enzymes SOD-3 and PRDX-3, and OMM transporter VDAC-1. Once in the cytoplasm, H_2O_2 activates stress-induced p38 MAPK signalling cascade necessary for the KLF-1 translocation to the nucleus and activation of the cytoprotective longevity assurance program in *C. elegans*. Our data further highlight a clear need for additional studies focusing more on mechanistic in-depth research on ROS signalling beyond oxidative stress that would extend across different species and could identify potential therapeutic targets for age-associated diseases.

4. Material and methods

4.1. Strains

Populations of *C. elegans* were cultured on *E.coli* OP50 bacteria-seeded NGM plates, according to standard protocols unless otherwise stated [88]. The following strains were used in this study: Bristol N2 (wild-type, N2), *isp-1(qm150);ctb-1(qm189)*, ATR4081 N2;*pvha-6::klf-1-yfp::prab-3::mCherry;rol-6(su1006)*, ATR4082 *isp-1(qm150);ctb-1(qm189)*;*pvha-6::klf-1-yfp::prab-3::mCherry;rol-6(su1006)*, ATR4030 N2; *pcyp-34a8::gfp;prab-3::mCherry*, ATR4026 *isp-1(qm150);ctb-1(qm189)*; *pcyp-34a8::gfp;prab-3::mCherry*, VC1151 *prdx-3(gk529)*, *VC289 prdx-2(gk169)* and JV2 N2;*prpl-17::Grx1-roGFP2;unc-119*. ATR4133 N2; atEx100 [*pmyo-3::roGFP2-ORP1;rol-6;prab-3::mCherry*] and ATR4135 N2; atEx100 [*pvha-6::roGFP2-ORP1;rol-6;prab-3::mCherry*], were generated by injecting the *pmyo-3::tomm20-roGFP2-ORP1* and *pvha-6::tomm20-roGFP2-ORP1* (40 ng/μl), respectively, *pGH8* (20 ng/μl) and *pRF4* (40 ng/μl) into N2 animals. Plasmid mixtures were injected using standard procedures [89]. ATR4133 and ATR4135 were crossed into *isp-1(qm150);ctb-1(qm189)* to create ATR4138 and ATR4139, respectively. JV2 was crossed into *isp-1(qm150);ctb-1(qm189)* to create ATR1045. ATR4141 N2; atEx100 [*pvha-6::klf-1-yfp(*K411 > A);prab-3::mCherry;rol-6(su1006)*] was generated by injecting the mutated constructs of *klf-1-yfp;* K411 > A (40 ng/μl), *pGH8* (20 ng/μl) and *pRF4* (40 ng/μl) into N2 animals. ATR4142 N2; atEx100 [*pvha-6::klf*-1-ha-*flag; prab-3::mCherry;rol-6(su1006)*] was generated by injecting the *klf*-1-ha-*flag* (40 ng/μl), *pGH8* (20 ng/μl) and *pRF4* (40 ng/μl) into N2 animals. ATR4142 was subsequently integrated by X-ray and outcrossed (ATR4146 strain) and crossed into *isp-1(qm150);ctb-1(qm189)* to create ATR4147 strain.

4.2. RNAi knockdown

RNAi knockdown was performed as described previously [90]. All genes for RNAi were obtained from the Ahringer RNAi library [90], or if stated from the Vidal RNAi library [91] and confirmed by sequencing. Clones are transformed into the *E. coli* HT115 (DE3) strain and enlisted in Table 1. Bacteria were grown in Luria broth medium to $OD_{595} = 0.5$, then 1 mM IPTG was added, and bacteria were induced for 3 h at 37 °C and consequently seeded on NGM plates containing 100 μg/ml ampicillin, 20 μg/ml tetracycline and 1 mM IPTG. Animals were treated with RNAi from hatching. For control, bacteria carrying the empty vector (EV) L4440 were used.

4.3. KLF-1 subcellular localization assay

KLF-1 subcellular localization was assayed by imaging worms on D1. For the KLF-1 subcellular localization experiments with drugs, the drugs were added to the plates at stated concentrations, and animals were exposed to the drugs from L4. The drug concentrations were: 2 μM antimycin a (AA, Sigma Aldrich), 10 μM Bortezomib (Bor, Sigma Aldrich), 5 mM Diamide (Sigma Aldrich), 5 μM FCCP (Sigma Aldrich), 25 mM malonate (Sigma Aldrich), 5 μM mitoparaquat (MitoPQ, Cayman), 2 μM myxothiazol (Myxo, Sigma Aldrich), 100 nM rotenone (Rot, Sigma Aldrich), 25 μM SB 203580 (Biomol), 25 μM thapsigargin (Tg, Sigma Aldrich), and 50 μM tunicamycin (Tu, Sigma Aldrich). For the experiments with vitamin C, 10 mM ascorbic acid (Vit c, Sigma Aldrich) was added directly to the NGM plates and worms were exposed from hatching. The antioxidant mtTEMPO (300 μM, Sigma Aldrich) and (SB205580 25 μM, Biomol) were added to the agar plates, and worms were transferred from L3 to D1 on these plates. Treatment with 5 mM dithiothreitol (DTT) and 10 mM H_2O_2 was performed by exposing worms for 30 min prior to imaging. KLF-1 presence in the nucleus was scored by YFP-positive punctae and divided into three categories: low nuclear localization (0–2 punctae), moderate nuclear localization (3–5 punctae), and high nuclear localization (>6 punctae).

4.4. Lifespan analysis

Worms were grown at 20 °C and exposed to RNAi from hatching unless otherwise stated. 300 μM mtTEMPO, 0.1 mM paraquat (PQ,

Table 1
RNAi clones from Ahringer or Vidal RNAi library.

Name	Sequence	Ahringer RNAi library
atp-5	C06H2.1	V-7J03
cco-1	F26E4.9	I-4L08
ctl-1	Y54G11A.6	II-9I01
ctl-2	Y54G11A.5	II-9G23
cyc-1	C54G4.8	I–3P14
klf-1	F56F11.3	III-1J15
nuo-2	T10E9.7	I-3M05
nsy-1	F59A6.1	II-4M01
pmk-1	B0218.3	IV-9P08
pmk-2	F42G8.3	IV-4G23
pmk-3	F42G8.4	IV-4I01
prdx-3	R07E5.2	III-2O03
prdx-6	Y38C1AA.11	IV-10F05
prx-5	C34C6	II-6G16
sek-1	R03G5.2	X-4E03
sod-1	C15F1.7	II-10114 E6 (Vidal)
sod-2	F10D11.1	I–4K13
sod-3	C08A9.1	X–8F07
wwp-1	Y65B4BR.4	I-10090 A1 (Vidal)
vdac-1	R05G6.7	IV-3D24

Sigma Aldrich), and 10 mM vitamin C treatments were performed from hatching. Worms were exposed their whole life to vitamin C, while mtTEMPO and PQ treatment lasted until D1. D1 was defined as day 1 of the lifespan. On day 0, 25 animals were transferred to each NGM plate, for a total of 100 worms per condition. Worms that escaped the plate or died due to protrusion or internal hatching were censored from the experiment. Compilation of lifespan data and statistical analysis are enlisted in Table S4.

4.5. Xenobiotic resistance assays

For vinblastine assay, eggs were incubated overnight in S-Complete medium. 20–30 synchronized L1 larvae per well were incubated in S-Complete medium with stated RNAi treatment and 1 mM IPTG and 20 nM Vit c. 100 μM vinblastine (Sigma Aldrich) was added per well, except for the untreated control wells. When the animals in the untreated control wells reached D1, the vinblastine treated animals were scored for developmental stages. Eight wells per condition were used and experiment was repeated three times.

For levamisole assay, 1 mM levamisole was directly added to the NGM plates. Worms were grown on stated RNAi or with vitamin C. On the fourth day of adulthood, worms were transferred on the levamisole plates and scored every 15 min for paralysis by prodding gently with the silver wire. Four plates per condition were used and experiment was repeated three times.

4.6. RNA isolation and qPCR

Animals were collected from one full plate and total RNA was isolated with Trizol (Invitrogen). DNAse treatment was achieved using DNA-free™, DNAse, and removal (Ambion, Life Technologies), according to the manufacturer's protocol. Amount of total RNA was quantified by spectrophotometry and 0.8 μg total RNA was reversely transcribed using the High-Capacity cDNA Reverse Transcription Kit (Applied Biosystems), with the following PCR conditions: 95 °C for 3 min, followed by 40 cycles of 95 °C for 5 s, 60 °C for 15 s. Detection of amplified products was performed using Brilliant III Ultra Fast SYBR Green qPCR Master Mix (Agillent Technologies) and normalization was against Y45F10D.4. Used primers are enlisted in Table 2. Data was represented using △△Ct and for each condition, five independent replicates were used.

4.7. Western blotting

Protein sample preparations were performed by collecting worms from three full plates and whasing them at least three times in M9 buffer. Worm pellet was frozen in liquid nitrogen and, depending on the amount of worm pellet, liquefied in 100–200 μM worm lysis buffer (25 mM Tris-HCL pH 7.4, 0.15 M NaCl, 1 mM EDTA, 1% NP-40, 0.5% SDS, 10 mM DTT and proteinase inhibitor cocktail (Roche)). PhosStop (Roche) was added when phospho-antibody was used. Samples were sonicated using the Bioruptor^{R} Sonication device (Diagenode) six times at 30/60 cycles.

Table 2
Primers.

Gene	Primer
cyp-13a7	Fw 5′-AAAAATGGCAATGGGACAAG-3′
	Rv 5′-AATACTTTGAATATCGGTAG-3′
cyp-13a11	Fw 5′-GCAAATTCTCGCCGTTGTAT-3′
	Rv 5′-TCGTCTCCTGATTCCCATCT-3′
cyp-14a1	Fw 5′-CCTTTCTTGGGGTCTCATCA-3′
	Rv 5′-AAGTAGCGGCTTGGATTGAA-3′
cyp-14a3	Fw 5′-CAGGCACTGGAGACAAATCA-3′
	Rv 5′-GCAAAAGAGAATGGGGGATT-3′
Y45F10D.4	Fw 5′-GTCGCTTCAAATCAGTTCAGC-3′
	Rv 5′-GTTCTTGTCAAGTGATCCGACA-3′

Samples were then centrifugaed for 15 min at 16,000×*g* at 4 °C and the supernatant was used. Protein concentration was measured with Bradford assay. Western blotting was performed using antibodies against ATP-1 (ATP5A, 1:2000 Abcam, #ab14748), GFP (1:2000, OriGene, #TP401), HSP-1 (HSC70 (B6), 1:4000, Santa Cruz, #sc-7298). LONP-1 (1:2000 Proteintech, #15440-1-AP), NUO-1 (NDUFV1, 1:2000 Proteintech, #11238-1-AP), NUO-2 (NDUFS3, 1:2000 MitoSciences, #MS112), Phospho-p38 MAPK (1:2000, Cell Signaling, #4511) and Phospho-(Ser/Thr) Phe (1:2000, Cell Signaling, #9631). Data were normalized to HSP-1.

4.8. Quantification of glutathione

Synchronized L4 and D1 worms were collected from five and three full plates, respectively, and washed three times with PBS buffer. Worms were subsequently resuspended in PBS, frozen in liquid nitrogen, thawed, and thoroughly lysed by sonification by the Bioruptor^{R} Sonication device, as previously described. Worm debris was removed by centrifugation. Supernatant was used for protein estimation, by Bradford assay, and total GSH, GSSG, and GSH/GSSG ratios were quantified using the GSH/GSSG-Glo assay kit (Promega) according to the manufacturer's protocol. For each condition, five biological replicates were analysed.

4.9. Site-directed mutagenesis

Site-directed mutagenesis was performed using QuickChange II XL Site-Directed Mutagenesis kit (Agilent Technologies) according to manufacturer's protocol with the following PCR conditions: 95 °C for 1 min, followed by 18 cycles of 95 °C for 50 s, 60 °C for 50 s and 68 °C for 90 s, afterwards 68 °C for 7 min and 4 °C until use. Template strand was construct *pvha-6::klf-1-yfp::prab-3::mCherry;rol-6(su1006)* and was digested by adding 1 μM *Dpn* I restriction enzyme for 1 h at 37 °C. Mutated constructs were transformed into XL10-Gold ultracompetent cells and confirmed by sequencing.

4.10. Co-immunoprecipitation (Co-IP) assay

Worms were harvested from at least twenty full plates and washed at least three times with 1x PBS. Worms were lysed by freezing in liquid nitrogen, adding modified RIPA buffer (50 mM Tris-HCL pH 7.4, 150 mM NaCl, 0.25% sodium-deoxycholate, 0.1% SDS, 1% NP-40, proteinase inhibitor cocktail and PhosStop) and sonicated in the Biorupter^{R}. Samples were centrifuged, supernatant collected, and CO-IP was performed using either GFP-Trap® Magnetic agarose (Proteintech) or Flag M2 antibody-coupled magnetic beads (Sigma Aldrich) at 4 °C for 2 h. Samples were eluted from the GFP-Trap® beads with SDS buffer (120 mM Tris/Cl pH 6.8, 20% glycerol, 4% SDS, 0.04% bromophenol blue, 10% βmercaptoethanol) and boiling. The samples were run on Western blot. Flag M2 beads were washed, and unbound proteins were eluted by elongation buffer (2 M Urea, 50 mM HEPES, 5 mM DTT). Then proteins were digested overnight at 37 °C by digestion buffer (2 M Urea, 50 mM HEPES, 5 mM DTT) with 50 ng LysC and 50 ng trypsin. Samples were acidified with formic acid and analysed by Mass Spectrometry.

4.11. Mass spectrometry of the Co-IP samples

All samples were analysed by the CECAD Proteomics Facility on a Q Exactive Plus Orbitrap mass spectrometer that was coupled to an EASY nLC (both Thermo Scientific) as previously described [92]. In brief, peptides were loaded with solvent A (0.1% formic acid in water) onto an in-house packed analytical column (50 cm ó 75 μm I.D., filled with 2.7 μm Poroshell EC120C18, Agilent). Peptides were chromatographically separated at a constant flow rate of 250 nL/min using the following gradient: 3–5% solvent B (0.1% formic acid in 80% acetonitrile) within 1.0 min, 5–30% solvent B within 40.0 min, 30–50% solvent B within 8.0

min, 50–95% solvent B within 1.0 min, followed by washing and column equilibration. The mass spectrometer was operated in data-dependent acquisition mode. The MS1 survey scan was acquired from 300 to 1750 *m/z* at a resolution of 70,000. The top 10 most abundant peptides were isolated within a 1.8 Th window and subjected to HCD fragmentation at a normalized collision energy of 27%. The AGC target was set to 5e5 charges, allowing a maximum injection time of 110 ms. Product ions were detected in the Orbitrap at a resolution of 35,000. Precursors were dynamically excluded for 10.0 s.

All mass spectrometric raw data were processed with Maxquant (version 1.5.3.8) using default parameters. Briefly, MS2 spectra were searched against the *C. elegans* WormBase ParaSite database (PRJNA13758, downloaded at: 15.04.2021) including a list of common contaminants. False discovery rates on protein and PSM level were estimated by the target-decoy approach to 1% (Protein FDR) and 1% (PSM FDR) respectively. The minimal peptide length was set to 7 amino acids and carbamidomethylation at cysteine residues was considered as a fixed modification. Oxidation (M) and Acetyl (Protein N-term) were included as variable modifications. The match-between runs option was enabled, LFQ quantification was enabled using default settings.

4.12. Microscopy

Worms were paralysed with 5 mM levamisole and mounted on 2% agarose pads. Images were captured using an Axiolmager Z.1 epifluorescence microscope, equipped with a Hammamatsu camera (OrcaR [2]) and AxioVision software 4.8, and analysed using Image J (National Institutes of Health).

4.13. Statistical analysis

To analyse statistical significance, a two-tailed unpaired Student's t-test, Chi-square test, or one-way ANOVA with Tukey post hoc test was used, unless otherwise stated. Error bars were represented as the standard error of the mean and significance was stated by $p < 0.05$ and represented by stars ($*p < 0.05$, $**p < 0.01$, $***p < 0.001$, $****p < 0.0001$). Unless otherwise stated, all experiments were performed three times independently of each other.

Acknowledgements

The authors wish to thank Dr. S. de Henau (University Medical Center, Utrecht) for providing us with the *tomm-20::roGFP2-Orp1* construct; the CECAD Proteomics Core and Dr. Jan-Wilm Lackmann for the analysis of co-immunoprecipitation assay; and CECAD Imaging Facility, Dr. Astrid Schauss and Dr. Christian Jüngst Center for Genomics (CCG) for their excellent technical support.

The work was supported by Aleksandra Trifunovic's grants from German Research Foundation (Deutsche Forschungsgemeinschaft - DFG) - SFB 1218 Projektnummer 269925409 and TR 1018/8–1 and Centre for Molecular Medicine Cologne, University of Cologne (C15).

Appendix A. Supplementary data

Supplementary data to this article can be found online at https://doi.org/10.1016/j.redox.2022.102533.

References

[1] D.E. Shore, G. Ruvkun, A cytoprotective perspective on longevity regulation, Trends Cell Biol. 23 (9) (2013) 409–420.
[2] E.S. Epel, G.J. Lithgow, Stress biology and aging mechanisms: toward understanding the deep connection between adaptation to stress and longevity, J Gerontol A Biol Sci Med Sci 69 (Suppl 1) (2014) S10–S16.
[3] J.M. Copeland, et al., Extension of Drosophila life span by RNAi of the mitochondrial respiratory chain, Curr. Biol. 19 (19) (2009) 1591–1598.
[4] C. Dell'agnello, et al., Increased longevity and refractoriness to Ca(2+)-dependent neurodegeneration in Surf1 knockout mice, Hum. Mol. Genet. 16 (4) (2007) 431–444.
[5] A. Ocampo, et al., Mitochondrial respiratory thresholds regulate yeast chronological life span and its extension by caloric restriction, Cell Metabol. 16 (1) (2012) 55–67.
[6] J. Feng, F. Bussiere, S. Hekimi, Mitochondrial electron transport is a key determinant of life span in Caenorhabditis elegans, Dev. Cell 1 (5Number) (2001) 633–644.
[7] S. Melov, et al., Extension of life-span with superoxide dismutase/catalase mimetics, Science 289 (5484) (2000) 1567–1569.
[8] A. Dillin, et al., Rates of behavior and aging specified by mitochondrial function during development, Science 298 (5602) (2002) 2398–2401.
[9] J.M. Van Raamsdonk, S. Hekimi, Reactive oxygen species and aging in Caenorhabditis elegans: causal or casual relationship? Antioxidants Redox Signal. 13 (12) (2010) 1911–1953.
[10] K.M. Holmström, T. Finkel, Cellular mechanisms and physiological consequences of redox-dependent signalling, Nat. Rev. Mol. Cell Biol. 15 (6) (2014) 411–421.
[11] W. Yang, S. Hekimi, A mitochondrial superoxide signal triggers increased longevity in Caenorhabditis elegans, PLoS Biol. 8 (12) (2010) e1000556.
[12] E. Munkacsy, S.L. Rea, The paradox of mitochondrial dysfunction and extended longevity, Exp. Gerontol. 56 (2014) 221–233.
[13] M. Ristow, S. Schmeisser, Extending life span by increasing oxidative stress, Free Radic. Biol. Med. 51 (2) (2011) 327–336.
[14] M. Herholz, et al., KLF-1 orchestrates a xenobiotic detoxification program essential for longevity of mitochondrial mutants, Nat. Commun. 10 (1) (2019) 3323.
[15] I. Bratic, et al., Mitochondrial DNA level, but not active replicase, is essential for Caenorhabditis elegans development, Nucleic Acids Res. 37 (6) (2009) 1817–1828.
[16] J.R. Vanfleteren, A. De Vreese, Rate of aerobic metabolism and superoxide production rate potential in the nematode Caenorhabditis elegans, J. Exp. Zool. 274 (2) (1996) 93–100.
[17] S.L. Rea, N. Ventura, T.E. Johnson, Relationship between mitochondrial electron transport chain dysfunction, development, and life extension in Caenorhabditis elegans, PLoS Biol. 5 (10) (2007) e259.
[18] E.L. Robb, et al., Selective superoxide generation within mitochondria by the targeted redox cycler MitoParaquat, Free Radic. Biol. Med. 89 (2015) 883–894.
[19] T.B. Sherer, et al., Mechanism of toxicity in rotenone models of Parkinson's disease, J. Neurosci. 23 (34) (2003) 10756–10764.
[20] D.V. Dervartanian, C. Veeger, Studies on succinate dehydrogenase. I. Spectral properties of the purified enzyme and formation of enzyme-competitive inhibitor complexes, Biochim. Biophys. Acta 92 (1964) 233–247.
[21] M. Davoudi, et al., A mouse model of mitochondrial complex III dysfunction induced by myxothiazol, Biochem. Biophys. Res. Commun. 446 (4) (2014) 1079–1084.
[22] E.C. Slater, The mechanism of action of the respiratory inhibitor antimycin, Biochim. Biophys. Acta 301 (July) (1973) 129–154.
[23] A.A. Starkov, G. Fiskum, Myxothiazol induces H(2)O(2) production from mitochondrial respiratory chain, Biochem. Biophys. Res. Commun. 281 (3) (2001) 645–650.
[24] F.L. Muller, et al., Architecture of the Q-o site of the cytochrome bc1 complex probed by superoxide production, Biochemistry 42 (21) (2003) 6493–6499.
[25] R. Benz, S. McLaughlin, The molecular mechanism of action of the proton ionophore FCCP (carbonylcyanide p-trifluoromethoxyphenylhydrazone), Biophys. J. 41 (3) (1983) 381–398.
[26] M. Xie, R. Roy, Increased levels of hydrogen peroxide induce a HIF-1-dependent modification of lipid metabolism in AMPK compromised C. elegans dauer larvae, Cell Metabol. 16 (3) (2012) 322–335.
[27] R.F. Wu, et al., Nox4-derived H2O2 mediates endoplasmic reticulum signaling through local Ras activation, Mol. Cell Biol. 30 (14) (2010) 3553–3568.
[28] A.C. Carrano, et al., A conserved ubiquitination pathway determines longevity in response to diet restriction, Nature 460 (7253) (2009) 396–399.
[29] A.C. Carrano, A. Dillin, T. Hunter, A krüppel-like factor downstream of the E3 ligase WWP-1 mediates dietary-restriction-induced longevity in caenorhabditis elegans, Nat. Commun. 5 (2014).
[30] X. Zhang, S.V. Srinivasan, J.B. Lingrel, *WWP1-dependent ubiquitination and degradation of the lung Kruppel-like factor, KLF2.* Elsevier 316 (1) (2004) 139–148/.
[31] C. Chen, et al., Human Kruppel-like factor 5 is a target of the E3 ubiquitin ligase WWP1 for proteolysis in epithelial cells, J. Biol. Chem. 280 (50) (2005) 41553–41561.
[32] A. Segref, S. Torres, T. Hoppe, A screenable in vivo assay to study proteostasis networks in Caenorhabditis elegans, Genetics 187 (4) (2011) 1235–1240.
[33] H. Sies, Strategies of Antioxidant Defense, 1993.
[34] A. Delaunay, A.-D. Isnard, M.B. Toledano, H2O2 sensing through oxidation of the Yap1 transcription factor, EMBO J. 19 (2000) 5157–5166.
[35] N. Kuksal, J. Chalker, R.J. Mailloux, Progress in understanding the molecular oxygen paradox - function of mitochondrial reactive oxygen species in cell signaling, Biol. Chem. 398 (11) (2017) 1209–1227.
[36] Y. Wang, et al., Superoxide dismutases: dual roles in controlling ROS damage and regulating ROS signaling, J. Cell Biol. 217 (6) (2018) 1915–1928.
[37] M. Fujii, et al., A novel superoxide dismutase gene encoding membrane-bound and extracellular isoforms by alternative splicing in Caenorhabditis elegans, DNA Res. 5 (1) (1998) 25–30.
[38] D. Gems, R. Doonan, Antioxidant defense and aging in C. elegans: is the oxidative damage theory of aging wrong? Cell Cycle 8 (11) (2009) 1681–1687.
[39] A. Perkins, et al., Peroxiredoxins: guardians against oxidative stress and modulators of peroxide signaling, Trends Biochem. Sci. 40 (8) (2015) 435–445.

[40] J.A. Arevalo, J.P. Vazquez-Medina, The role of peroxiredoxin 6 in cell signaling, Antioxidants 7 (12) (2018).
[41] M. Oláhová, et al., A redox-sensitive peroxiredoxin that is important for longevity has tissue- and stress-specific roles in stress resistance, Proc. Natl. Acad. Sci. U.S.A. 105 (50) (2008) 19839–19844.
[42] M. Olá Hová, et al., A Redox-Sensitive Peroxiredoxin that Is Important for Longevity Has Tissue-And Stress-specific Roles in Stress Resistance, 2008.
[43] L.H. Ma, C.L. Takanishi, M.J. Wood, Molecular mechanism of oxidative stress perception by the Orp1 protein, J. Biol. Chem. 282 (43) (2007) 31429–31436.
[44] L.P. Roma, et al., Mechanisms and applications of redox-sensitive green fluorescent protein-based hydrogen peroxide probes, Antioxidants Redox Signal. 29 (6) (2018) 552–568.
[45] B.P. Braeckman, et al., Vivo detection of reactive oxygen species and redox status in Caenorhabditis elegans, Antioxidants Redox Signal. 25 (10) (2016) 577–592.
[46] S. De Henau, et al., Mitochondria-derived H2O2 promotes symmetry breaking of the C. elegans zygote, Dev. Cell 53 (3) (2020) 263–271 e6.
[47] A. Muller, et al., Systematic in vitro assessment of responses of roGFP2-based probes to physiologically relevant oxidant species, Free Radic. Biol. Med. 106 (2017) 329–338.
[48] G.P. Bienert, J.K. Schjoerring, T.P. Jahn, Membrane transport of hydrogen peroxide, Biochim. Biophys. Acta 1758 (8) (2006) 994–1003.
[49] D.N. DeHart, et al., Opening of voltage dependent anion channels promotes reactive oxygen species generation, mitochondrial dysfunction and cell death in cancer cells, Biochem. Pharmacol. 148 (2018) 155–162.
[50] R.M. Cordeiro, Molecular dynamics simulations of the transport of reactive oxygen species by mammalian and plant aquaporins, Biochim. Biophys. Acta 1850 (9) (2015) 1786–1794.
[51] Z.X. Ni, et al., Structural and evolutionary divergence of aquaporins in parasites (Review), Mol. Med. Rep. 15 (6) (2017) 3943–3948.
[52] T. Uozumi, et al., Voltage-dependent anion channel (VDAC-1) is required for olfactory sensing in Caenorhabditis elegans, Gene Cell. 20 (10) (2015) 802–816.
[53] S. Kosugi, et al., Systematic identification of cell cycle-dependent yeast nucleocytoplasmic shuttling proteins by prediction of composite motifs, Proc. Natl. Acad. Sci. U.S.A. 106 (25) (2009) 10171–10176.
[54] J. Kaczynski, T. Cook, R. Urrutia, Sp1- and Kruppel-like transcription factors, Genome Biol. 4 (2) (2003) 206.
[55] J.M. Shields, V.W. Yang, Two potent nuclear localization signals in the gut-enriched Kruppel-like factor define a subfamily of closely related Kruppel proteins, J. Biol. Chem. 272 (29) (1997) 18504–18507.
[56] K. Melen, et al., Importin alpha nuclear localization signal binding sites for STAT1, STAT2, and influenza A virus nucleoprotein, J. Biol. Chem. 278 (30) (2003) 28193–28200.
[57] A. Corcoran, T.G. Cotter, Redox regulation of protein kinases, FEBS J. 280 (9) (2013) 1944–1965.
[58] A. Sagasti, et al., The CaMKII UNC-43 activates the MAPKKK NSY-1 to execute a lateral signaling decision required for asymmetric olfactory neuron fates, Cell 105 (2) (2001) 221–232.
[59] M. Tanaka-Hino, et al., SEK-1 MAPKK Mediates Ca 2+ Signaling to Determine Neuronal Asymmetric Development in Caenorhabditis elegans, 2002, pp. 56–62.
[60] J.M. Hoyt, et al., The SEK-1 p38 MAP kinase pathway modulates Gq signaling in caenorhabditis elegans, G3: Genes, Genomes, Genetics 7 (9) (2017) 2979–2989.
[61] C.K. Sen, Cellular thiols and redox-regulated signal transduction, Curr. Top. Cell. Regul. 36 (2000) 1–30.
[62] C.S. Chen, et al., WWP-1 is a novel modulator of the DAF-2 insulin-like signaling network involved in pore-forming toxin cellular defenses in Caenorhabditis elegans, PLoS One 5 (3) (2010).
[63] A.C. Carrano, A. Dillin, T. Hunter, A Kruppel-like factor downstream of the E3 ligase WWP-1 mediates dietary-restriction-induced longevity in Caenorhabditis elegans, Nat. Commun. 5 (2014) 3772.
[64] M.D. Conkright, M.A. Wani, J.B. Lingrel, Lung krüppel-like factor contains an autoinhibitory domain that regulates its transcriptional activation by binding WWP1, an E3 ubiquitin ligase, J. Biol. Chem. 276 (31) (2001) 29299–29306.
[65] H.M. Cocheme, M.P. Murphy, Complex I is the major site of mitochondrial superoxide production by paraquat, J. Biol. Chem. 283 (4) (2008) 1786–1798.
[66] W. Yang, S. Hekimi, Two modes of mitochondrial dysfunction lead independently to lifespan extension in Caenorhabditis elegans, Aging Cell 9 (3) (2010) 433–447.
[67] A.M. Pickering, et al., Oxidative stress adaptation with acute, chronic, and repeated stress, Free Radic. Biol. Med. 55 (2013) 109–118.
[68] T.J. Schulz, et al., Glucose restriction extends Caenorhabditis elegans life span by inducing mitochondrial respiration and increasing oxidative stress, Cell Metabol. 6 (4) (2007) 280–293.
[69] A. Zuin, et al., Lifespan extension by calorie restriction relies on the Sty1 MAP kinase stress pathway, EMBO J. 29 (5) (2010) 981–991.
[70] C. Yee, W. Yang, S. Hekimi, The intrinsic apoptosis pathway mediates the pro-longevity response to mitochondrial ROS in C. elegans, Cell 157 (4) (2014) 897–909.
[71] M. Ranjan, et al., Repression of the mitochondrial peroxiredoxin antioxidant system does not shorten life span but causes reduced fitness in Caenorhabditis elegans, Free Radic. Biol. Med. 63 (2013) 381–389.
[72] S. Penkov, et al., A metabolic switch regulates the transition between growth and diapause in C. elegans, BMC Biol. 18 (1) (2020).
[73] I. Bratic, et al., Mitochondrial DNA level, but not active replicase, is essential for Caenorhabditis elegans development, Nucleic Acids Res. 37 (6) (2009) 1817–1828.
[74] A. Delaunay, et al., A thiol peroxidase is an H2O2 receptor and redox-transducer in gene activation, Cell 111 (4) (2002) 471–481.
[75] M.N. Hoehne, et al., Spatial and temporal control of mitochondrial H2 O2 release in intact human cells, EMBO J. 41 (7) (2022) e109169.
[76] B. Zhou, et al., Mitochondrial permeability uncouples elevated autophagy and lifespan extension, Cell 177 (2) (2019) 299–314, e16.
[77] G.P. Bienert, et al., Specific aquaporins facilitate the diffusion of hydrogen peroxide across membranes, J. Biol. Chem. 282 (2) (2007) 1183–1192.
[78] B. Canovas, A.R. Nebreda, Diversity and versatility of p38 kinase signalling in health and disease, Nat. Rev. Mol. Cell Biol. 22 (5) (2021) 346–366.
[79] M.T. Harreman, et al., Regulation of nuclear import by phosphorylation adjacent to nuclear localization signals, J. Biol. Chem. 279 (20) (2004) 20613–20621.
[80] J.D. Nardozzi, K. Lott, G. Cingolani, Phosphorylation meets nuclear import: a review, Cell Commun. Signal. 8 (2010) 32.
[81] H. Inoue, et al., The C. elegans p38 MAPK pathway regulates nuclear localization of the transcription factor SKN-1 in oxidative stress response, Gene Dev. 19 (19) (2005) 2278–2283.
[82] M. Kondo, et al., Effect of oxidative stress on translocation of DAF-16 in oxygen-sensitive mutants, mev-1 and gas-1 of Caenorhabditis elegans, Mech. Ageing Dev. 126 (6–7) (2005) 637–641.
[83] M. Saitoh, et al., Mammalian thioredoxin is a direct inhibitor of apoptosis signal-regulating kinase (ASK) 1, EMBO J. 17 (9) (1998) 2596–2606.
[84] M. Chamoli, et al., Polyunsaturated fatty acids and p38-MAPK link metabolic reprogramming to cytoprotective gene expression during dietary restriction, Nat. Commun. 11 (1) (2020).
[85] E. Munkácsy, et al., DLK-1, SEK-3 and PMK-3 are required for the life extension induced by mitochondrial bioenergetic disruption in C. elegans, PLoS Genet. 12 (7) (2016).
[86] T. Tralau, A. Luch, The evolution of our understanding of endo-xenobiotic crosstalk and cytochrome P450 regulation and the therapeutic implications, Expet Opin. Drug Metabol. Toxicol. 9 (12) (2013) 1541–1554.
[87] P.B. Danielson, The cytochrome P450 superfamily: biochemistry, evolution and drug metabolism in humans, Curr. Drug Metabol. 3 (6) (2002) 561–597.
[88] S. Brenner, The genetics of Caenorhabditis elegans, Genetics (77) (1974) 71–94.
[89] C.C. Mello, et al., Efficient gene transfer in C.elegans: extrachromosomal maintenance and integration of transforming sequences, EMBO J. 10 (12) (1991) 3959–3970.
[90] R.S. Kamath, et al., Systematic functional analysis of the Caenorhabditis elegans genome using RNAi, Nature 421 (6920) (2003) 231–237.
[91] J.F. Rual, et al., Toward improving Caenorhabditis elegans phenome mapping with an ORFeome-based RNAi library, Genome Res. 14 (10B) (2004) 2162–2168.
[92] S. Koyuncu, et al., Rewiring of the ubiquitinated proteome determines ageing in C. elegans, Nature 596 (7871) (2021) 285–290.